Available online at www.sciencedirect.com
ScienceDirect
Journal of Power Sources 173 (2007) 707–711
JOURNAL OF POWER SOURCES
www.elsevier.com/locate/jpowsour

Electrochemical and high temperature physicochemical properties of orthorhombic $LiMnO_2$

Janina Molenda [a,*], Mariusz Ziemnicki [a], Jacek Marzec [a], Wojciech Zając [a], Marcin Molenda [b], Mirosław Bućko [a]

[a] *Faculty of Materials Science and Ceramics, AGH University of Science and Technology, al. Mickiewicza 30, 30-059 Krakow, Poland*
[b] *Faculty of Chemistry, Jagiellonian University, ul. Ingardena 3, 30-060 Krakow, Poland*

Available online 21 May 2007

Abstract

In this work we report the investigation of the structural and the electrical properties of orthorhombic $LiMnO_2$ in a wide temperature range in air and in high purity argon (N5). Also we present a correlation between the electrical and the electrochemical properties of the material upon lithium deintercalation. Moreover, its chemical stability against $LiPF_6$ based liquid electrolyte at elevated temperatures was measured and compared with other cathode materials.

High temperature investigations revealed occurrence of phase transitions. During heating in oxidizing and in inert atmosphere orthorhombic phase decomposes into $LiMn_2O_4$ and $LiMn_2O_3$. The conducted experiments also pointed to the instability of orthorhombic $LiMnO_2$ during electrochemical lithium deintercalation. Both electrical conductivity and thermoelectric power of deintercalated samples altered substantially. DSC measurements proved high thermal stability of $LiMnO_2$ based cathode material in contact with commercial liquid electrolyte.
© 2007 Elsevier B.V. All rights reserved.

Keywords: Li-ion batteries; $LiMnO_2$; $LiMn_2O_4$; Spinel; Thermal stability

1. Introduction

Lithium manganese oxide $LiMnO_2$ with orthorhombic structure (o-$LiMnO_2$) is a compound from a group of new, promising cathode materials for Li-ion batteries. It exhibits a high gravimetric capacity (290 mAh g^{-1}), high potential of an electrochemical reaction versus lithium anode and is environmentally benign [1]. However, this material is structurally unstable at high temperatures and is relatively difficult to synthesize [2]. The transport properties of $LiMnO_2$ are not sufficiently known, despite they are crucial in terms of the electrochemical performance.

The goal of this work was to investigate structural, transport and electrochemical properties of the orthorhombic $LiMnO_2$ and material after electrochemical delithiation.

2. Experimental

Orthorhombic $LiMnO_2$ was obtained by a coprecipitation method. Lithium and manganese (II) acetates were used as the precursors. The substrates in stoichiometric proportions were dissolved in deionized water. Concentrated ammonia solution (25 wt.%) was a precipitation agent. The obtained sol, after condensation, was dried at 363 K to yield xerogel, which was subsequently calcinated in air, in the temperature range 523–573 K, for 24 h. The obtained brownish-black product was powdered, pelleted, and again calcinated in flowing argon at 1123 K for 20 h. After that it was quenched in order to preserve high temperature crystal structure.

The crystal structure was determined by the X-ray diffraction method using PHILIPS X'Pert diffractometer operating with Cu Kα radiation. The high temperature phase transitions were investigated by a thermogravimetric method together with a high temperature XRD studies.

The electrochemical behavior of $LiMnO_2$ was studied in the $Li/Li^+/Li_yMnO_2$ cells. In the tests a custom-made electrochemical cells were used, with a metallic lithium anode and 1 M $LiPF_6$ solution in 1:1:1 wt. EC:DEC:DMC solvent. Whatman glass microfiber filters were used as well as Cellgard microporous separators. For electrochemical measurements cathode materials were mixed with 20 wt.% graphite, about 30 mg cm^{-2} of active material was used. Charge/discharge curves were measured at room temperature using Kest Electronics 32 K amperostat.

* Corresponding author. Tel.: +48 12 6172522; fax: +48 12 6172522.
E-mail address: molenda@agh.edu.pl (J. Molenda).

0378-7753/$ – see front matter © 2007 Elsevier B.V. All rights reserved.
doi:10.1016/j.jpowsour.2007.05.054

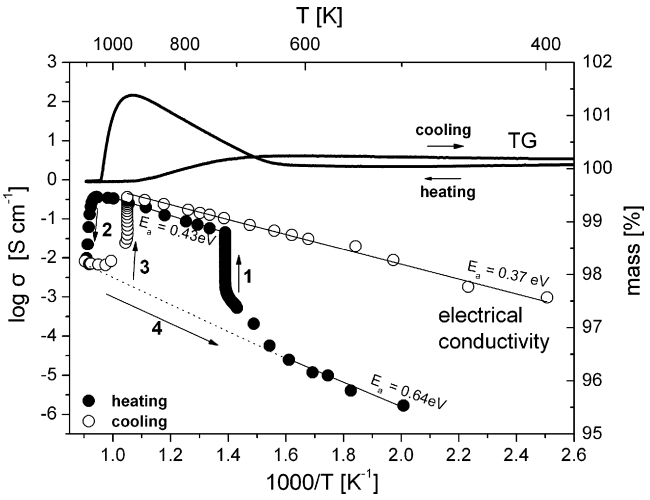

Fig. 1. Electrical conductivity of the o-$LiMnO_2$ (heating/cooling rate 0.2 K min^{-1}) and the corresponding TG curve (heating/cooling rate 2.5 K min^{-1}) measured in high purity argon (N5).

Applied current density was 20 μA cm^{-2}. The phase composition of the cathode material with different delithiation degree (the content of an orthorhombic and a spinel phase) was estimated on the basis of refining XRD patterns using Rietveld method.

A differential scanning calorimetry (DSC) and thermogravimetric (TG) methods were applied to evaluate the thermal stability of starting and deintercalated $LiMnO_2$. Both measurements were conducted using Mettler-Toledo 851^e apparatus. Mass of the samples was 50 mg ± 5% in TG measurement and 15 mg in DSC measurements.

3. Results and discussion

The results obtained by means of the XRD method confirmed that samples were single-phase, orthorhombic $LiMnO_2$. Estimated grain size of the obtained samples was of the order of a few μm.

Fig. 1 presents the electrical conductivity of o-$LiMnO_2$ in cycle of heating and cooling in high purity argon (p_{O_2} = 10^{-5} atm) with 0.2 K min^{-1} rate. Moreover, a corresponding TG curve is included in Fig. 1. As can be seen, the variations of electrical conductivity are very complex. The structural examination of the specimens taken in the characteristic points of the electrical conductivity hysteresis indicates that the quenched, orthorhombic structure of $LiMnO_2$, present at room temperature, becomes unstable at elevated temperatures. The orthorhombic phase in the temperature range of 500–600 K has the electrical conductivity thermally activated with the activation energy equal 0.64 eV. At about 720 K the electrical conductivity suddenly increases by 10^3 and a simultaneous increment of the sample mass is observed, which is associated with the decomposition of o-$LiMnO_2$:

$$3LiMnO_2 + \tfrac{1}{2}O_2 = LiMn_2O_4 + Li_2MnO_3 \quad (1)$$

One of the reactants in reaction (1) is residual oxygen from flowing (N5) argon gas. Higher conductivity of the spinel phase, $LiMn_2O_4$, is the reason for the observed significant increase in the conductivity (Fig. 1, arrow 1). The high conductivity of 10^{-1} S cm^{-1} and the activation energy of 0.43 eV observed at temperatures 720–1100 K are characteristic for the manganese spinel $LiMn_2O_4$ [3], conductivity of Li_2MnO_3 is lower by several orders of magnitude. However, above 1100 K and low oxygen pressure 10^{-5} atm the manganese spinel is not stable [3]. Consequently the reaction (1) proceeds to the left, which is reflected by a sudden drop of conductivity and the corresponding mass loss (arrow 2 in Fig. 1), related to the formation of the orthorhombic $LiMnO_2$ phase. The orthorhombic phase, which has much lower conductivity, is stable in these conditions. By quenching the orthorhombic phase the high-temperature structure is preserved and the conductivity variations follow the arrow 4 in Fig. 1 Slow cooling of the high-temperature orthorhombic phase leads again to the decomposition of $LiMnO_2$ into manganese spinel $LiMn_2O_4$ and Li_2MnO_3 at about 950 K (arrow 3 in Fig. 1, reaction (1)).

Fig. 2a and b present TG and DTG (differential TG) curves for o-$LiMnO_2$ measured, consequently in air and in high purity argon. Generally, the shapes of both curves are quite alike. This indicates that mechanism of the decomposition is similar in both cases. The observed reaction rate was higher for the samples heated in air, though the total amount of accumulated oxygen was smaller. This leads to the conclusion that the surface of the sample, which was in a contact with air becomes passivated,

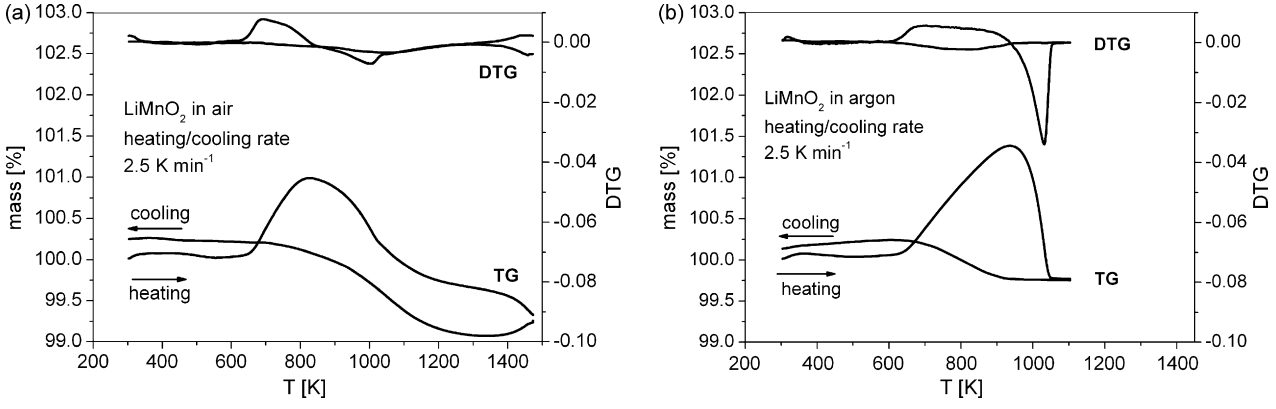

Fig. 2. TG and DTG curves of $LiMnO_2$ sample heated in (a) air and in high purity argon (N5) (b).

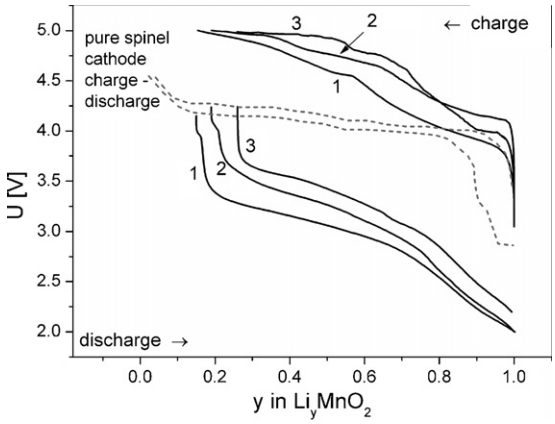

Fig. 3. First three charge/discharge cycles of the $Li/Li^+/Li_yMnO_2$ cell at a current density of 20 μA cm^{-2} [7]. The first charge/discharge cycle for pure spinel cathode is attached for comparison (dashed line). *y* stands for average amount of lithium in the cathode material [mol/mol].

due to fast oxidation and a creation of a gas-tight layer of the Li_2MnO_3 phase, with a low oxygen diffusion coefficient. In the argon atmosphere ($p_{O_2} \sim 10^{-5}$ atm) a very slow oxidation proceeds according to the (Eq. (1)) and the passivation process does not occur, thus the observed mass uptake due to oxidation is higher than that for the air atmosphere.

In Fig. 3 the first three charge/discharge curves for $Li/Li^+/Li_yMnO_2$ cell are presented. During the first cycle, at a current density of 20 μA cm^{-2}, about 80% of the theoretical capacity is achieved, during the third cycle it fades about 10% and is equal to 200 mA g^{-1}. For comparison, the first charge/discharge curve for $Li/Li^+/Li_yMn_2O_4$ is also presented.

The analysis of subsequent discharge curves character leads to the important conclusion concerning stability of orthorhombic $LiMnO_2$ during electrochemical delithiation/lithiation process. The observed increase of the cell potential during consecutive discharge cycles cannot be associated with properties of o-$LiMnO_2$ phase. Cyclic lithium deintercalation/intercalation destabilizes orthorhombic structure and contributes to its transformation to the cubic spinel phase. Similar behavior was observed by other researchers [4–6].

In Fig. 4 the comparison of open circuit voltage (OCV) curves of the cell containing Li_yMnO_2 based cathode and, for comparison, pure $Li_yMn_2O_4$ spinel cathode are presented.

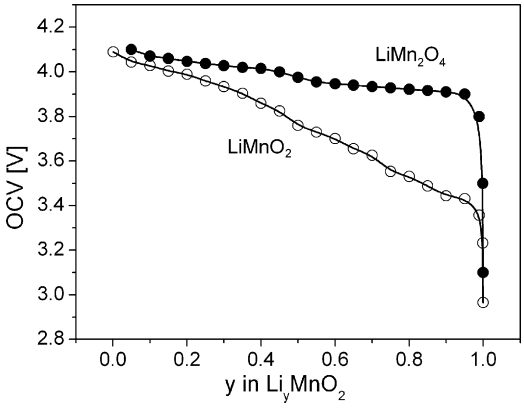

Fig. 4. Comparison of the $LiMnO_2$ and $LiMn_2O_4$ OCV curves.

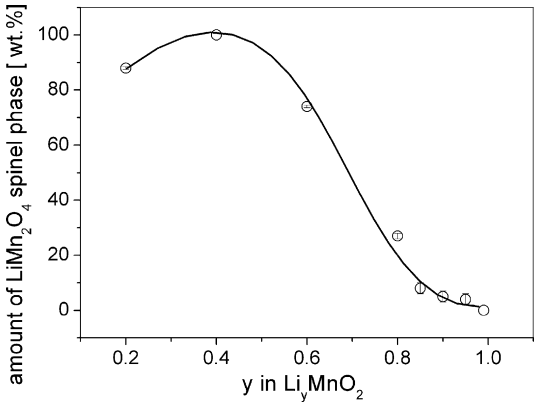

Fig. 5. $LiMn_2O_4$ spinel phase contribution in composite cathode.

Comparing the charge/discharge curves (Fig. 3) to the OCV (Fig. 4), large polarization during charge/discharge processes is observed. It can be ascribed to the high resistance of the cathode material [7]. In contrast with $Li^+/Li_yMn_2O_4$ cathode, a stepwise change of the electrode potential is observed for Li^+/Li_yMnO_2 cathode during lithium deintercalation, suggesting that the electronic structure of orthorhombic $LiMnO_2$ significantly differs from the electronic structure of $LiMn_2O_4$, in which isolated Mn^{3+} and Mn^{4+} states exist.

The X-ray studies carried for the deintercalated Li_yMnO_2 based cathode materials (Fig. 5) at different deintercalation stage, obtained during the first cell charge, prove an increasing contribution of the spinel-like phase up to 100% for deintercalation degree $y_{Li} = 0.4$. For lower lithium contents probably tetragonal Mn_3O_4 appears. Similar result was obtained by Kötschau and Dahn [5].

Charge/discharge curves analysis and structural studies showed that observed phase transition (o-$LiMnO_2 \leftrightarrow LiMn_2O_4$) is reversible. However, kinetics of this process is complex and depends on parameters of charge/discharge, such as current density, relaxation time, and requires further examinations.

Fig. 6a and b present evolution of the lattice constants for orthorhombic Li_yMnO_2 and $Li_yMn_2O_4$ spinel phases during lithium electrochemical deintercalation. The nonlinear behavior of parameters evolution is observed, denoting a complex mechanism of the cathode process. As the obtained spinel lattice constant values decrease with lithium deintercalation progress, the newly created spinel phase is electrochemically active and undergoes delithiation (beside orthorhombic phase delithiation) during the cell charge process. The observed lattice constants are between 8.22 and 8.11 Å. These values are rather low as compared with delithiated manganese spinel prepared with high temperature method with lattice constant between 8.25 and 8.18 Å. This implies that in electrochemical process a heavily defected spinel-like ($Li_{1-x}Mn_2O_4$) phase is created. A similar lattice constant was observed for $LiMn_2O_4$ spinel prepared with sol–gel process [8,9].

On the basis of the XRD measurements and the charge/discharge curves analysis the process of lithium deintercalation may be divided into two concurrent stages and described

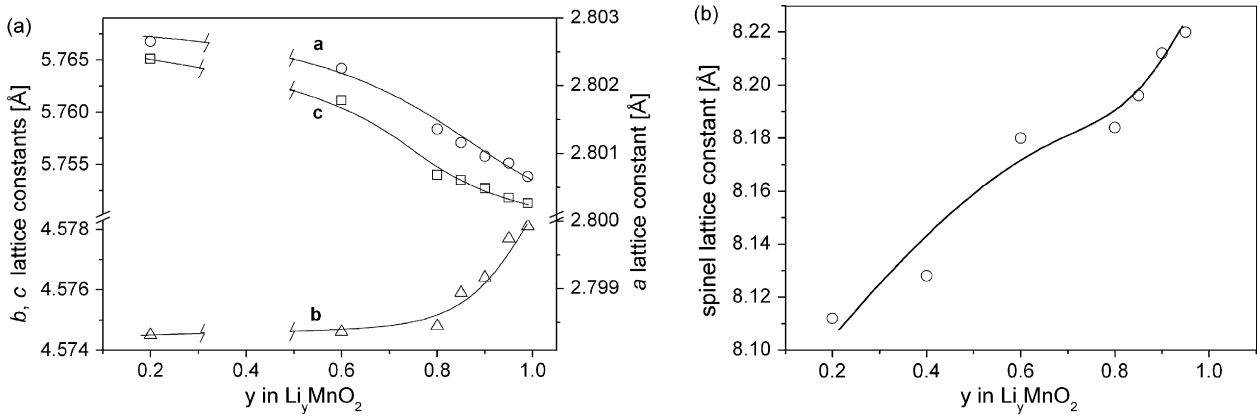

Fig. 6. Lattice constants of (a) orthorhombic Li_yMnO_2 and (b) spinel during first charge cycle as a function of deintercalation stage (◯, *a*: lattice constant, △, *b*: lattice constant, □, *c*: lattice constant).

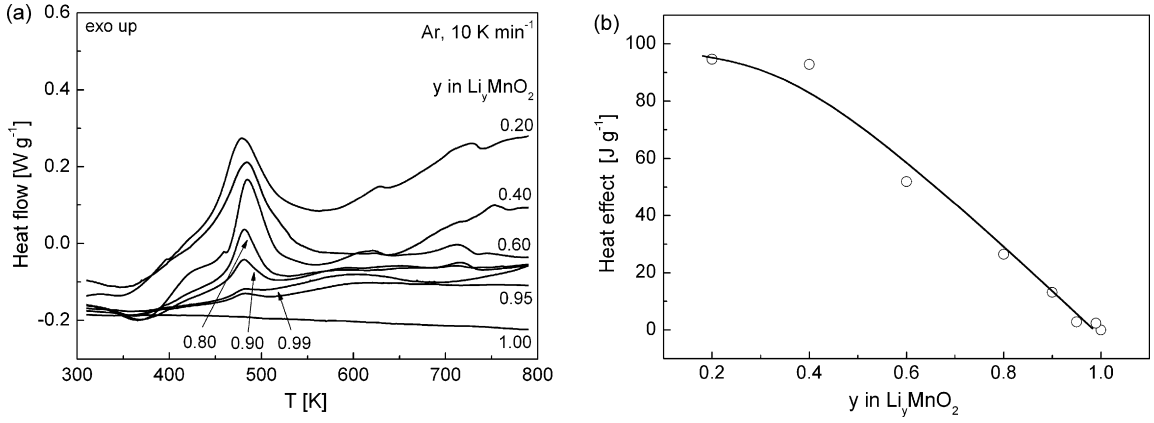

Fig. 7. (a) DSC measurements and (b) integral heat effects for composite cathode material at different deintercalation stages.

qualitatively with the following equations:

$$4LiMnO_2 = LiMn_2O_4 + Li_{2-x}Mn_2O_4 + (1+x)Li \quad (2)$$

$$LiMn_2O_4 = Li_{1-x}Mn_2O_4 + xLi \quad (3)$$

In this region a cause of the electrochemical reaction is the deintercalation of the orthorhombic $LiMnO_2$. The newly created phases are: the spinel phase $LiMn_2O_4$ and delithiated, defected orthorhombic phase with the $Li_{2-x}Mn_2O_4$ stoichiometry. The defected $Li_{2-x}Mn_2O_4$ phase is isostructural with the orthorhombic $LiMnO_2$. The deintercalation process of the $LiMn_2O_4$ phase also occurs (Eq. (3)), thus its lattice constant decreases with an increase of the delithiation stage (Fig. 6b). However, the maximum concentration of the spinel-like phase is observed for $y_{Li} = 0.4$ (Fig. 5), while the orthorhombic phase is not present. Further deintercalation process of the material leads to formation of manganese oxide with the structure analogous to tetragonal Mn_3O_4, exhibiting similar XRD pattern as the orthorhombic phase.

The observed unusual OCV curve shape can be assigned to the equilibrium of the two phases present in the cathode material: $Li_{2-x}Mn_2O_4$ and $Li_{1-x}Mn_2O_4$. A relatively large potential drop during charge/discharge processes points to a considerable cathode material polarization. This may be caused by a kinetic limitation in reaching the equilibrium state or even by a creation of temporary, metastable phases.

A chemical stability in relation to a liquid electrolyte of a cathode material in charged (oxidized) state is a very important feature especially from commercial point of view. Fig. 7a presents the results of DSC measurements taken for cathode material being in contact with commonly used commercial lithium liquid electrolyte ($LiPF_6$ 1 M, solvent EC:DEC:DMC

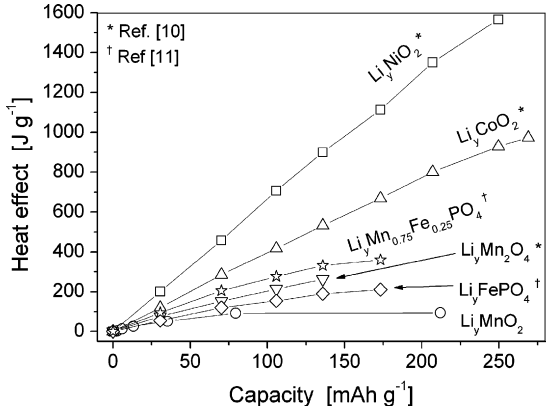

Fig. 8. Comparison of the heat effects measured with DSC method for different cathode materials for Li-ion batteries.

1:1:1) at different deintercalation stages (during first charge process). The observed integral heat effect increases with the increasing deintercalation stage (Fig. 7b). This can be explained on the basis of increasing oxidation state of manganese in cathode material.

The observed values of heat effects for deintercalated $LiMnO_2$-based cathode materials are much lower than the ones obtained for other cathode materials used for Li-ion batteries. As a result, prepared composite cathode material is the safest material among others. It is clearly presented in Fig. 8, which shows the heat effects of the reaction with an electrolyte for different cathode materials [10,11].

4. Conclusions

The attractive electrochemical and thermal properties of the obtained cathode material based on the orthorhombic $LiMnO_2$ result from the partial transformation to defected $Li_{1-x}Mn_2O_4$ spinel structure. Moreover, this lithium manganese spinel, created by the electrochemical route at room temperature, exhibits improved chemical stability as compared with $LiMn_2O_4$ prepared in the high temperature synthesis.

Acknowledgement

This work is supported by AGH University of Science and Technology under Statutory Researches 11.11.160.363.

References

[1] T. Ohzuku, A. Ueda, T. Hirai, Chem. Express 7 (1992) 193–196.
[2] R.J. Gumow, M.M. Thackeray, J. Electrochem. Soc. 141 (1994) 1178–1182.
[3] J. Molenda, K. Świerczek, W. Kucza, J. Marzec, A. Stokłosa, Solid States Ionics 123 (1999) 155–163.
[4] L. Croguennec, P. Deniard, R. Brec, P. Biensan, M. Broussely, Solid State Ionics 89 (1996) 127–137.
[5] I.M. Kötschau, J.R. Dahn, J. Electrochem. Soc. 145 (1998) 2672–2677.
[6] G.X. Wang, P. Yao, S. Zhong, D.H. Bradhurst, S.X. Dou, H.K. Liu, J. Appl. Electrochem. 29 (1999) 1423–1426.
[7] J. Molenda, M. Ziemnicki, M. Molenda, M. Bućko, J. Marzec, Mater. Sci. Poland 24 (2006) 73–83.
[8] M. Molenda, R. Dziembaj, E. Podstawka, L.M. Proniewicz, J. Phys. Chem. Solids 66 (2005) 1761–1768.
[9] M. Molenda, R. Dziembaj, W. Łasocha, C. Rudowicz, L.M. Proniewicz, E. Podstawka, H. Ohta, Jpn. J. Appl. Phys. 45 (2006) 5132–5137.
[10] Z. Zhang, D. Fouchard, J.R. Rea, J. Power Sources 70 (1998) 16–20.
[11] G. Li, H. Azuma, M. Tohda, J. Electrochem. Soc. 149 (2002) A743–A747.